Anomalous magnetic behavior of Ba_{2}CoO_{4} with isolated CoO_{4} tetrahedra

Qiang Zhang, Guixin Cao, Feng Ye, Huibo Cao, Masaaki Matsuda, D. A. Tennant, Songxue Chi, S. E. Nagler, W. A. Shelton, Rongying Jin, E. W. Plummer, and Jiandi Zhang

Phys. Rev. B **99**, 094416 — Published 14 March 2019

DOI: 10.1103/PhysRevB.99.094416

Anomalous Magnetic Behavior in Ba_2CoO_4 with Isolated CoO_4 Tetrahedra

Qiang Zhang[1,2], Guixin Cao[1], Feng Ye[2], Huibo Cao[2], Masaaki Matsuda[2], D. A. Tennant[2], Songxue Chi[2], S. E. Nagler[2], W.A. Shelton[3], Rongying Jin[1], E. W. Plummer[1], and Jiandi Zhang[1*]

[1]Department of Physics and Astronomy, Louisiana State University, Baton Rouge, Louisiana 70803, USA

[2]Neutron Scattering Division, Oak Ridge National Laboratory, Oak Ridge, Tennessee 37831, USA

[3]Cain Department of Chemical Engineering, Louisiana State University, Baton Rouge, Louisiana 70803, USA

Abstract

The dimensionality of the electronic and magnetic structure of a given material is generally predetermined by its crystal structure. Here, using elastic and inelastic neutron scattering combined with magnetization measurements, we find unusual magnetic behavior in three-dimensional (3D) Ba_2CoO_4. In spite of isolated CoO_4 tetrahedra, the system exhibits a 3D noncollinear antiferromagnetic order in the ground state with an anomalously large Curie-Weiss temperature of 110 K compared to T_N = 26 K. More unexpectedly, spin dynamics displays quasi-2D spin wave dispersion with an unusually large spin gap, and 1D magnetoelastic coupling. Our results indicate that Ba_2CoO_4 is a unique system for exploring the interplay between isolated polyhedra, low-dimensional magnetism, and novel spin states in oxides.

PACS number(s): 75.47.Lx, 75.25.-j, 75.30.Ds, 75.80.+q

*Corresponding author: jiandiz@lsu.edu

It is anticipated that low-dimensional magnetism in a material is directly related to its low dimensional crystal structure [1], such as in cuprates [2], Fe-based pnictides [3], ferromagnetic semiconductor $CrSiTe_3$ [4], double-layer perovskite $Sr_3(Ru_{1-x}Mn_x)_2O_7$ [5], or Weyl semimetals in $YMnBi_2$ [6], etc. In these materials, the quasi-two-dimensional (2D) magnetism originates from the clearly layered crystal structure where the nearest-neighbor (NN) M-M distance (where M is a transition metal element) along the interlayer direction is much larger than that within the layer, which yields a very weak interlayer magnetic interaction [1-6]. It would be of great interest to explore whether quasi-2D magnetism could be realized in a nonlayered compound involving comparable NN M-M distances in a crystallographically 3D system. The identification of such a system may shed light on the microscopic origin of quansi-2D magnetism.

Different from other well-studied cobaltates with the Co ion in an octahedral environment, monoclinic Ba_2CoO_4 [7-8] has a 3D crystallographic structure with *isolated* tetrahedral CoO_4 without any corner-, edge- or face-sharing [Fig. 1(a)]. Naively one would expect that the spin correlation in Ba_2CoO_4 is very weak, presumably dictated by spin dipole-dipole interaction with energy $U \approx \frac{1}{(137)^2}\left(\frac{a_0}{4}\right)^3 Ry$ [9]. Using the shortest Co-Co distance of 4.67 Å, we estimate $U \sim$ 0.01 meV, implying that any magnetic ordering would happen below 0.1 K. Yet, Ba_2CoO_4 exhibits AFM ground state below $T_N \approx 26$ K [8,10,11] with an anomalously high Curie-Weiss temperature ($|\theta| \sim 110$ K), which is > 4 times larger than T_N [11]. The large $|\theta|/T_N$ ratio could be a result of spin frustration [12, 13] or low dimensional magnetism [14] existing in the system. To complicate any interpretation of magnetism is the fact that the reported magnetic structures are inconsistent with each [10, 15]. Boulahya *et al.* [10] reported a canted AFM order in the *bc* plane based on powder neutron diffraction measurements. In contrast, muon spin rotation and relaxation (μ^+SR) experiments [15] found that the magnetic moment is basically along the *a* axis.

In addition, spin dimer analysis [16] for the magnetic coupling in Ba_2CoO_4 has no indication of quasi-2D magnetism. Super-superexchange (SSE) mechanism [16-19], which describes spin interactions beyond direct Co-O-Co superexchange pathways, was proposed to be responsible for the magnetic interaction in Ba_2CoO_4. However, there is no experimental confirmation to date.

Here, we demonstrate different dimensionality between static and dynamical magnetism in Ba_2CoO_4. The system exhibits a 3D noncollinear AFM order with buckled zig-zag chains along the *b* axis below T_N = 26 K but 1D magnetoelastic coupling occurs along the *a* direction, despite well-separated CoO_4 tetrahedra [Fig. 1(a)]. However, the spin waves (SWs) display a quasi-2D character with dispersion in the *ab*-plane. An anomalous spin gap (~2.55 meV) comparable to the SW bandwidth reflects a large magnetic anisotropy. The magnon dispersion relation analyzed using the linear SW theory reveals large anisotropic magnetic interactions. The results can be interpreted in terms of a frustrated network of Co-O···O-Co spin exchange pathways where the overlapping oxygen *p*-orbitals determine the amplitude of magnetic interactions. The uniaxial magnetoelastic effect is the evidence of a certain spin-lattice coupling to stabilize the 3D AFM order against the spin frustration.

Ba_2CoO_4 crystals were synthesized using the floating zone method [20]. Single-crystal neutron diffraction was used to determine the structure of Ba_2CoO_4 [21,22], revealing a monoclinic structure with space group $P2_1/n$ (No. 14) at 5 K as illustrated in Fig. 1(a). There are 4 Co atoms in one crystalline unit cell. This result is consistent with previous neutron and x-ray diffraction measurements [10,11]. Temperature (*T*)-dependence of the magnetization (M) for Ba_2CoO_4 in a field of 0.1 T is shown in Fig. 1(b) for three principal directions. Note that M decreases with increasing temperature above T_N with no anisotropy. Below T_N = 26 K, M_a drops much faster than M_c, while M_b increases after a small drop. This indicates anisotropic magnetism

below T_N, with the AFM configuration along both the *a* and *c* directions, but ferromagnetic (FM)-like alignment along the *b* direction. The rapid decrease of M_a below T_N implies that the moment direction mainly points to the *a* axis. Fitting to the inverse susceptibility (*H*//*a*) at the high-temperature linear portion of the curve with the Curie-Weiss law ($\chi = \frac{C}{T+\theta}$) yields a Curie-Weiss temperature $\theta \approx$ 109 K, consistent with the previous reports [10,11].

Figures 1(c) and (d) show the temperature dependences of the lattice constants determined by measuring the *Q* scans through the nuclear peaks (400), (020) and (004) of neutron diffraction, given there is a negligible change in the monoclinic beta angle <0.6° between RT and 5 K. Above T_N, the lattice constants in all three directions show identical *T* dependence with thermal expansion coefficient $\alpha \sim 9\times10^{-6}$ K^{-1} (close to the value for glass of 7.6×10^{-6} K^{-1} [23]). However, the lattice constant *a* exhibits anomalous behavior with an abrupt and nonlinear drop below T_N, indicating strong magnetoelastic coupling in this specific direction. The *T*-dependence of the lattice constant *a* (Fig. 1(c)) scales inversely with the magnetic order parameter shown in Fig. 2(a).

Magnetic peaks with a commensurate propagation wavevector $\boldsymbol{k}$ = (-1/2, 0, 1/2) appear below T_N in the neutron diffraction due to long range magnetic ordering. The *T*-dependent peak intensity of the magnetic Bragg peak (-1/2, 1, 1/2) in Fig. 2(a) shows an AFM transition at T_N. As illustrated in Fig. 2(b), the overall magnetic structure is AFM with an ordered moment of 2.69(4) μ_B/Co, consisting of 16 Co spins in the magnetic unit cell. The magnetic unit cell is $2a\times b\times 2c$ with respect to the crystalline unit cell with $|\boldsymbol{m}_a|$ = 2.377 μ_B, $|\boldsymbol{m}_b|$ = 1.128 μ_B, and $|\boldsymbol{m}_c|$ = 0.586 μ_B, respectively. All the Co spins are antiparallel along the *a* and *c* axes, but double-stripe type parallel configuration along the *b*-axis, consistent with the magnetization measurements. The

moments primarily point along the *a* axis and alternatively canted with a canting angle to the *b* axis ~ ±25^{o} and to the *c* axis ~ ±13^{o} [21,24,25].

The spin dynamics is investigated using inelastic neutron scattering. The inset of Fig. 2(a) shows the spectra of the constant-*Q* energy scan at two magnetic zone centers, (1/2, 0, 1/2) and (1/2, 1, 1/2) at 5 K. A spin gap of $\Delta \approx 2.55(3)$ meV is observed at 5 K and disappears at T_N, confirming its magnetic origin. This is in stark contrast to the isotropic nature of the high spin state Co^{4+} (S=5/2, L=0, $e^2t_2^3$) reported previously [7-8,10-11,15] due to the full quenching of the orbital angular momentum and consequently the absence of any spin gap. The AFM ordered moment of 2.69(4) μ_B is also much lower than $5\mu_B$ expected for high spin state of Co^{4+} but close to $3\mu_B$ for the intermediate spin state of Co^{4+} (S=3/2). Both indicate that the ground state of Ba_2CoO_4 is in the intermediate spin (IS) state Co^{4+} (S=3/2, $L\neq0$, $e^3t_2^2$). While the IS state of Co^{4+} was frequently observed in cobaltites when Co is in an octahedral environment, the IS state of Co^{4+} in the tetrahedral environment seems very rare. Early theoretical calculations [26] indicated that all the IS (S=3/2) states of $3d^5$ cation in the tetrahedral environment may not be stable. Recently, Kauffmann et al. [27] proposed that the off-centering of O atoms from its ideal tetrahedral positions may induce the intermediate spin state of tetrahedral Co^{4+} ion. The x-ray absorption spectroscopy and/or theoretical calculations are needed, in order to investigate the microscopic origin of the possible IS state in Ba_2CoO_4.

Figures 2(c-f) display the contour plots of $S(Q, E)$, determined from the constant-*Q* energy scans along the [*H* 0 0], [0 *K* 0], [0 0 *L*] and diagonal [*H* 0 *H*] direction at 5 K (see Note 3 in SM). Two SW branches appear along the [*H* 0 0] and [*H* 0 *H*] directions with the more dispersive being the high-energy branch. These two branches nearly merge along the [0 *K* 0] and [0 0 *L*] directions. Surprisingly, the magnon bandwidth is less than 3 meV, close to the spin gap value of

~2.6 meV. In contrast, both the energy and intensity of the SW along the [0 0 L] direction show negligible dispersion, indicating that Ba_2CoO_4 exhibits a surprising quasi-2D magnetism.

To identify the observed SW modes and quantitatively obtain the magnetic exchange parameters, we have performed the linear SW calculations using the SpinW package [29] with an effective Heisenberg-like Hamiltonian given by

$$H = \sum_{i \neq j} J_{ij} \vec{S}_i \cdot \vec{S}_j + \sum_i A_i \vec{S}_i^2 \qquad (1)$$

where $\vec{S}_i$ denotes the spin of magnetic Co ion at site i, J_{ij} describes the magnetic exchange coupling constant between spin-pairs at site i and j, $\sum_{i \neq j}$ indicates summation over pairs of spins, and A_i is the diagonal element of the 3×3 single-ion anisotropy matrix. The best fitting values of the exchange parameters SJ_{ij} and anisotropy parameter SA as listed in Table I. Compared to SA_b and SA_c, the anisotropy parameter SA_a is extremely small, consistent with the ordered moment mainly aligned to a axis. Due to the large spin gap, it is impossible to fit the experimental data of spin waves without large anisotropy term. It is worthwhile noting that the spin dimer analysis proposed in Ref. 16 does not include single-ion anisotropy.

Figure 3(a) illustrates the magnetic structure, doubling of the *ab* plenary lattice structure (PLS) and the important exchange constants used in the fitting of spin waves. Considering only Co sites for two stacking PLSs shown in Fig. 3(a), each Co atom is surrounded by six NN Co atoms with comparable Co-Co distances. The two adjacent PLSs are not identical, thus there are two quasi-2D PLSs in the magnetic unit cell alternating along the c axis and connected by the exchange coupling of $J_\perp$. Figure 3(b) shows the projection of one quasi-2D PLS onto the *ab* plane. The spin configuration within each PLS is collinear but the spin ordering between the adjacent PLSs is not, forming an overall noncollinear AFM order. For each quasi-2D PLS, the

spins form a buckled AFM double-chain structure with strong exchange couplings [J_1, and J_1', see Fig. 3(b)] along the *b* direction. Six NN pairs (including four intra-PLS pairs, J_1, J_1', J_2, J_2', and two equivalent inter-PLS pairs, $J_\perp$) and one next nearest neighbor (NNN) pair J_3, marked in Fig. 3(a-b), plus three diagonal elements (A_i) of single-ion anisotropy matrix, are included to fit the dispersion. Using the fitting *J* values and the determined magnetic structure, the corresponding SW spectra $S(Q, E)$, along the four measured directions in the reciprocal space in units (*H,K,L*) are simulated as shown in Fig. 3(c-f), which are in good agreement with the experimental data in Fig. 2(c-f).

The important messages from the SW fitting and simulation are: 1) The inter-PLS $J_\perp$, which characterizes the dispersion along the *c* axis is less than 5% of the intra-PLS J_1, J_1', J_2, J_2', and J_3, reflecting the quasi-2D magnetism. 2) Spins form AFM zigzag chains along the *b* axis due to the strong magnetic interactions J_1 and J_1'. These chains are coupled through the unexpected strong NNN interaction J_3, comparable with J_1 and J_1'. 3) Within one PLS [see Fig. 3(b)], there are two distinct distorted triangles marked by grey (J_1, J_2 with J_3) and blue (J_1', J_2' with J_3), respectively. Although all the fitted J_{ij} values are positive, i.e., AFM, the spin configurations associated with J_2 and J_2' are FM [see Fig. 3(b)], therefore, this lifts spin frustration within these triangles and leads to long-range magnetic order. 4) The anisotropic coefficients in the *b* and *c* directions are three orders larger than that in the *a* direction. This indicates that spins prefer to be aligned along the *a* axis with a collinear configuration. Such energy more favorable state is obtained because of the 1D magnetoelastic effect [Fig. 1(c)]. The 1D magnetoelastic coupling along *a* direction at T_N may be associated with the details of the exchange interaction [30,31]. In this case, J_3 needs to be large enough to stabilize such a

magnetic structure against spin frustration in two triangular lattices. The magnetoelastic effect below T_N exactly reflects the correlation of J_3 and lattice constant in the *a* direction.

The quasi-2D magnetism in Ba_2CoO_4 is novel and fundamentally different from the conventional quasi-2D magnetism compounds [2-6]: i) The crystal structure is 3D with isolated CoO_4 tetrahedra, lacking well separated magnetic and nonmagnetic layers as in conventional quasi-2D magnetism compounds; ii) There are two distinct stackings repeated along the *c* axis in Ba_2CoO_4. The spin arrangement is collinear within each of stacking, but they are noncollinear between these two stackings connected by a negligible $J_\perp$ to be responsible for the quasi-2D magnetism; iii) Although intra-PLS Co-Co distance of $J_\perp$ is shorter than those of the intra-PLS couplings J_1', J_2'and J_3, the magnitude of $J_\perp$ between the two stackings is two orders smaller.

The static and dynamic magnetic behavior of magnetism in Ba_2CoO_4 are schematically summarized in Fig. 4(a), 1D spin-lattice coupling, quasi-2D spin waves and 3D magnetic order. Given the fact that CoO_4 tetrahedra are isolated with large Co-Co spacing (> 4.662 Å), there should be little direct exchange interaction between Co atoms. Thus, the spin-spin interaction via indirect spin exchange pathways ought to be considered. For Ba_2CoO_4, indirect spin interactions may take place through Co- O···O-Co or Co-O-Ba-O-Co exchange paths. The exchange path of Co- O···O-Co is referred as the super-superexchange (SSE) mechanism [16,19], in contrast to conventional superexchange model [32]. The sign and the magnitude of interactions via Co-O···O-Co are not necessarily governed by the direct Co-Co distances, but by the overlap of orbitals along Co- O···O-Co, especially the overlap of their *p*-orbitals of the non-bonding O···O in the vicinity of the van der Waals distance [16-19]. Given the O···O distances and the Co-O···O or O···O-Co angles are critical in determining the overlap of the O *p*-orbitals, it is important to compare the obtained magnetic exchange parameters with the corresponding crystallographic

parameters. Thus, we determined the O···O distances and the Co-O···O or O···O-Co angles based on our Rietveld refinements of neutron diffraction results. As shown in Figs. 4(b-d) and Ref. [33], the inter-PLS Co-Co tetrahedra are less coplanar than intra-PLS Co-Co tetrahedra, which does not favor the overlap of the O *p*-orbitals. In the two exchange pathways Co-O_1···O_3-Co and Co-O_1···O_2-Co for $J_\perp$ [see Fig. 4(c)], the O···O distances are comparable to those for J_1', J_2' and J_3 [see Figs. 4(b) and (d)], but the ∠ Co-O···O and ∠O···O-Co angles are close to 90^o and smaller than the corresponding angles for J_1', J_2' and J_3, thus leading to a much weaker $J_\perp$ based on SSE model (see Note 4 in SM for more details).

In summary, we have investigated magnetic structure, magnetic interactions and magnetoelastic coupling in Ba_2CoO_4 with isolated CoO_4 tetrahedra. The system exhibits a 3D noncollinear long-range AFM order below T_N = 26 K with magnetic moment primarily along the *a*-axis. The spin excitation spectra reveal a quasi-2D SW dispersion with an unusually large spin gap ~ 2.55(3) meV and the *T*-dependent lattice constants clearly illustrate a strong 1D magnetoelastic effect along *a*-axis. The concurrence of 3D lattice structure, 3D noncollinear magnetic structure, quasi-2D spin waves dispersion, 1D magnetoelastic coupling, and the unusual intermediate spin state of Co^{4+} in a tetrahedral environment make Ba_2CoO_4 a unique system for exploring novel magnetism. Our work may open a new avenue to investigate quasi-2D magnetism in nonlayered structure involving isolated coordinate polyhedron and could be an important stimulus to explore the very rare intermediate spin state in the $3d^5$ cations such as Mn^{2+}, Fe^{3+}, Co^{4+} in the tetrahedral environment.

Acknowledgments: We would like to thank Zhentao Wang and Sándor Tóth for helpful discussions. This work was primarily supported by the U.S. Department of Energy under EPSCoR Grant No. DE-SC0012432 with additional support from the Louisiana Board of Regents. Use of the high flux isotope reactor at the Oak Ridge National Laboratory, was supported by the US Department of Energy, office of Basic Energy Sciences, Scientific User Facilities Division.

Table I. The optimal parameters obtained by fitting experimental SW dispersions with the linear spin wave theory (see details in the main text), compared with corresponding Co-Co distances.

	SJ_1	SJ_1'	SJ_2	SJ_2'	$SJ_\perp$	SJ_3	SA_a	SA_b	SA_c
Value (meV)	1.29(6)	1.13(4)	0.58(6)	0.45(4)	0.015(8)	1.11(5)	0.5×10^{-3}	0.52(8)	0.46(7)
Co-Co distance (Å)	4.662	5.323	4.797	5.442	5.186	5.884			

References

1. J. G. Bednorz, and K. A. Müller, Z. Phys. B **64**, 189 (1986).

2. B. Keimer, S. A. Kivelson, M. R. Norman, S. Uchida and J. Zaanen, Nature **518**, 179 (2015)

3. Yoichi Kamihara, Takumi Watanabe, Masahiro Hirano, and Hideo Hosono, J. Am. Chem. Soc. **130**, 3296 (2008).

4. T. J. Williams, A. A. Aczel, M. D. Lumsden, S. E. Nagler, M. B. Stone, J.-Q. Yan, and D. Mandrus, Phys. Rev. B **92**, 144404 (2015).

5. Qiang Zhang, Feng Ye, Wei Tian, Huibo Cao, Songxue Chi, Biao Hu, Zhenyu Diao, David A. Tennant, Rongying Jin, Jiandi Zhang, and Ward Plummer, Phys. Rev. B, **95**, 220403(R) (2017).

6. Sergey Borisenko, Daniil Evtushinsky, Quinn Gibson, Alexander Yaresko, Timur Kim, MN Ali, Bernd Buechner, Moritz Hoesch, Robert J Cava, arXiv :1507.04847 (2015).

7. Von Hj. Mattausch, and Hk. Muller-Buschbaum, Anorg. Allg. Chem. **386**, 1 (1971).

8. K. Boulahya, M. Parras, A. Vegas, and J. M. González-Calbet, Solid State Sciences **2**, 57 (1998).

9. N. W. Ashcroft and N. D. Mermin, Solid State Physics, page 673, Holt, Rinehart and Winston, New York (1976).

10. K. Boulahya, M. Parras, J. M. González-Calbet, U. Amador, J. L. Martínez, and M. T. Fernández-Díaz, Chem. Mater. **18**, 3898 (2006).

11. R. Jin, Hao Sha, P. G. Khalifah, R. E. Sykora, B. C. Sales, D. Mandrus, and Jiandi Zhang, Phys. Rev. B **73**, 174404 (2006).

12. A. P. Ramirez, MRS Bull. **30**, 447 (2005).

13. A. A. Zvyagin, Low Temperature Phys. **39**, 901 (2013).

14. L. J. de Jongh and A. R. Miedema, Adv. Phys. **23**, 1 (1974).

15. Peter L. Russo, Jun Sugiyama, Jess H. Brewer, Eduardo J. Ansaldo, Scott L. Stubbs, Kim H. Chow, Rongying Jin, Hao Sha, and Jiandi Zhang, Phys. Rev. B **80,** 104421 (1609).

16. H. -J. Koo, K. -S. Lee, and M. -H. Whangbo, Inorg. Chem., **45** (26), 10743 (2006).

17. M. -H. Whangbo, D. Dai, and H, -J. Koo, Solid State Sci. **7**, 827 (2005).

18. M, -H. Whangbo, H, -J. Koo, and D. Dai, J. Solid State Chem. **176**, 417 (2003).

19. H.- J. Koo, M., H. Whangbo, and K. -S. Lee, J. Solid State Chem. **169**, 143 (2002).

20. See Supplemental Material at XXXXX for details of experimental methods.

21. See Supplemental Material at XXXXX for details of crystalline and magnetic structure determination with neutron-diffraction.

22. B. C. Chakoumakos, H. Cao, F. Ye, A. D. Stoica, M. Popovici, M. Sundaram, W. Zhou, J. S. Hicks, G. W. Lynn and R. A. Riedel, J. Appl. Crystallogr. **44**, 655 (2011).

23. P. Hidnert, Journal of Research of the National Bureau of Standards **52**, 311 (1954).

24. A. S. Wills, Physica B **276–278**, 680 (2000).

25. J.M. Perez-Mato, S.V. Gallego, E.S. Tasci, L. Elcoro, G. de la Flor, and M.I. Aroyo, Annu. Rev. Mater. Res. **45**, 217 (2015).

26. Michel Pouchard, Antoine Villesuzanne, and Jean-Pierre Doumerc, Comptes Rendus Chimie **6**, 135 (2003).

27. Matthieu Kauffmann, Olivier Mentré, Alexandre Legris, Sylvie Hébert, Alain Pautrat, and Pascal Roussel, Chem. Mater. **20**, 1741 (2008).

28. See Supplemental Material at XXXXX for details of spin wave dispersion determination.

29. S. Toth and B. Lake, J. Phys.: Condens. Matter **27**, 166002 (2015).

30. M. C. Cross and D. S. Fisher, Phys. Rev. B **19**, 402 (1979).

31. Y. Tokura, S. Seki and N. Nagaosa, Rep. Prog. Phys. **77**, 076501 (2014).

32. P. W. Anderson, Phys. Rev. **79**, 350 (1950).

33. See Supplemental Material (Tables SIV and SV) at XXXXX for details of interatomic distance, angles of the CoO_4 tetrahedra and geometrical parameters of the SSE pathways.

34. See Supplemental Material at XXXXX for details of possible magnetic exchange pathways.

35. R. Sinclair, H. D. Zhou, M. Lee, E. S. Choi, G. Li, T. Hong, and S. Calder, Phys. Rev. B **95**, 174410 (2017).

36. Angela Möller, Ngozi E. Amuneke, Phillip Daniel, Bernd Lorenz, Clarina R. de la Cruz, Melissa Gooch, and Paul C. W. Chu, Phys. Rev. B **85**, 214422 (2012).

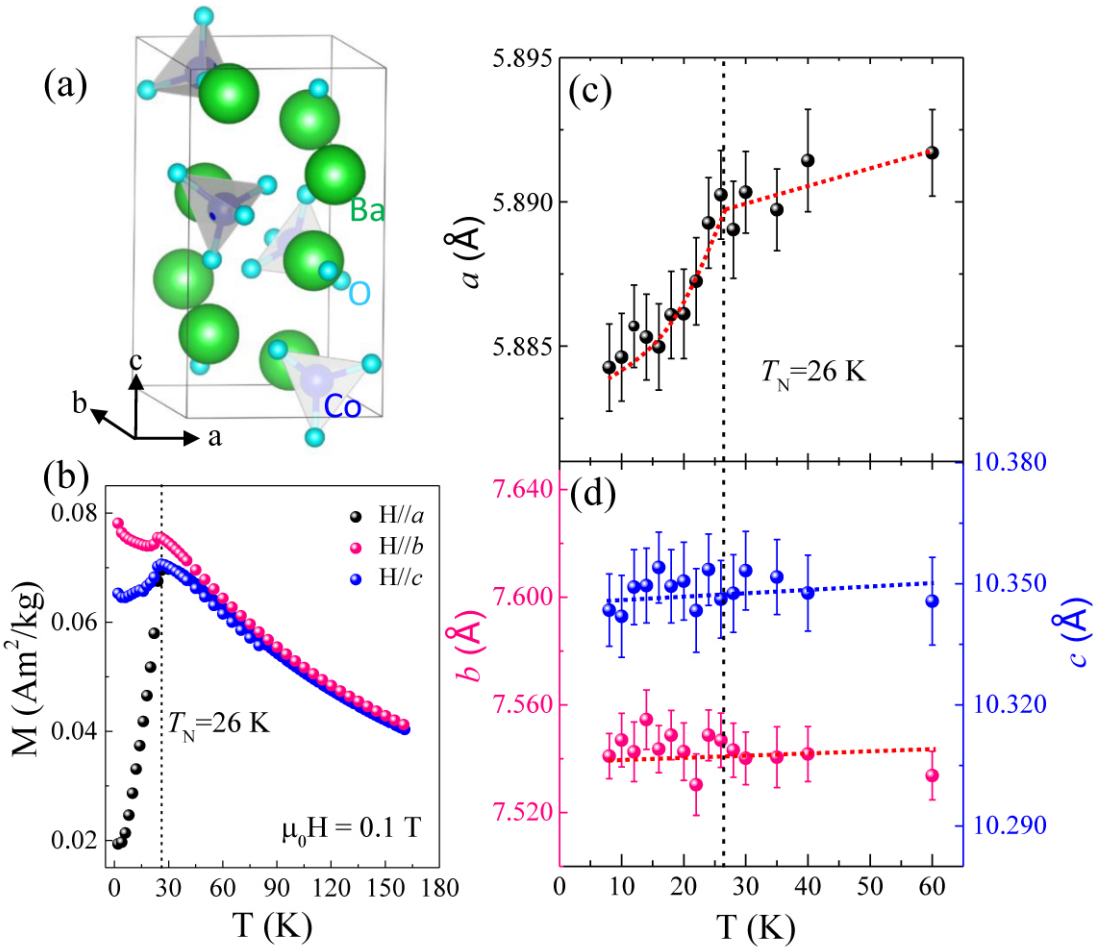

Fig. 1. Structural information of Ba_2CoO_4. (a) A 3D view of the monoclinic unit cell for $Ba_8Co_4O_{16}$ (simplified as Ba_2CoO_4). (b) *T*-dependence of the magnetization curves for Ba_2CoO_4 in a field of 0.1 T applied parallel to the crystalline *a*-, *b*- and *c*-axes. (c) and (d) *T*-dependence of the lattice constants *a, b* and *c*. The vertical dashed line shows the location of AFM transition temperature T_N.

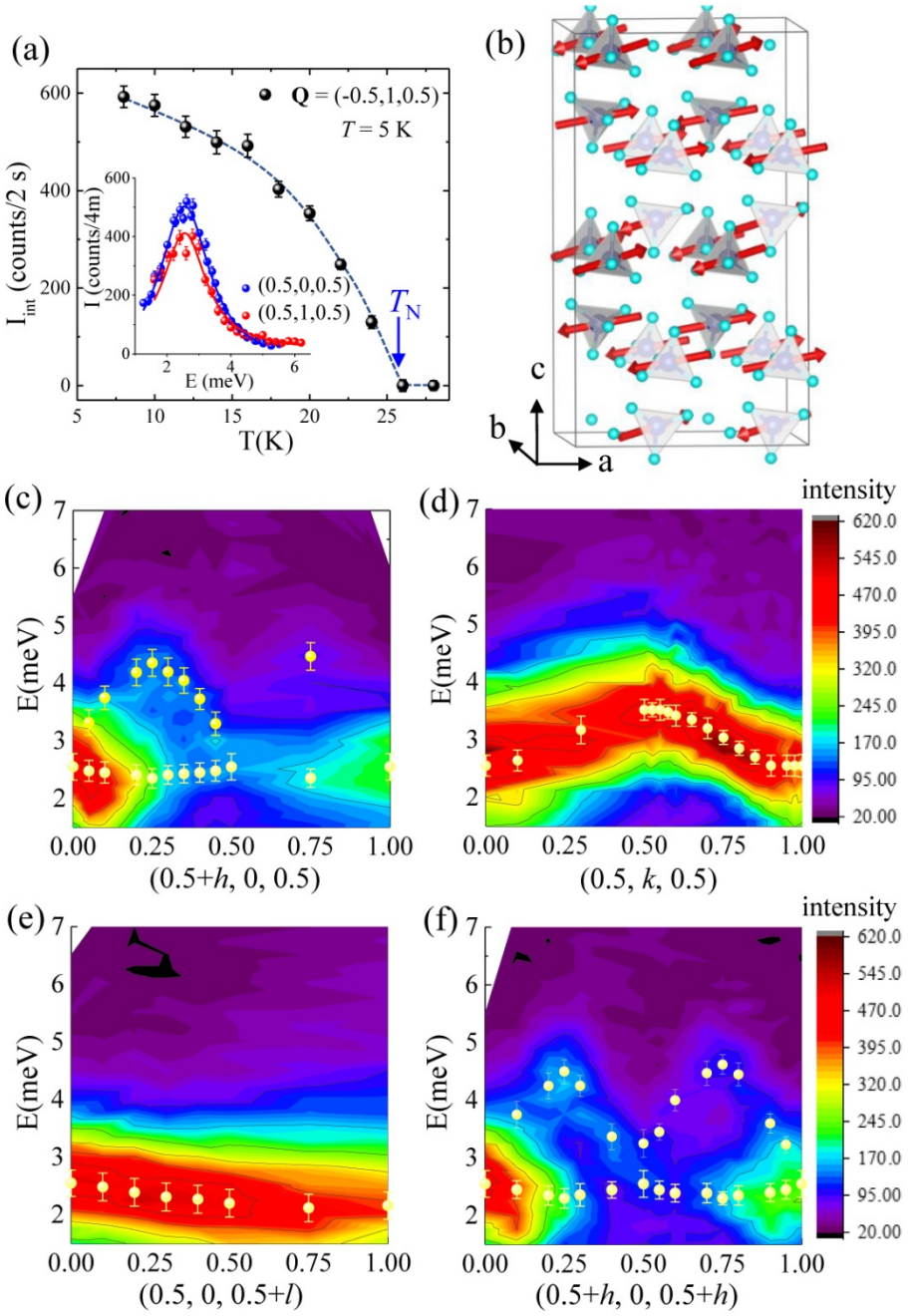

Fig. 2. (a) Order parameter of magnetic (-0.5,1,0.5) peak. The inset shows the spin gap at two magnetic zone centers (0.5,0,0.5) and (0.5,1,0.5). (b) The 3D graphic representation of the determined magnetic structure of Ba_2CoO_4 at 5 K within $2a\times1.3b\times2c$ unit cells (note that one magnetic unit cell is $2a\times b\times2c$ unit cells). (c)-(f) Experimental S(Q, E) contour plots along the [H 0 0], [0 K 0], [0 0 L] and [H 0 H] directions in the r.l.u. The dot symbols show the experimental spin-wave dispersions obtained by the fits to the raw data (see details in the main text).

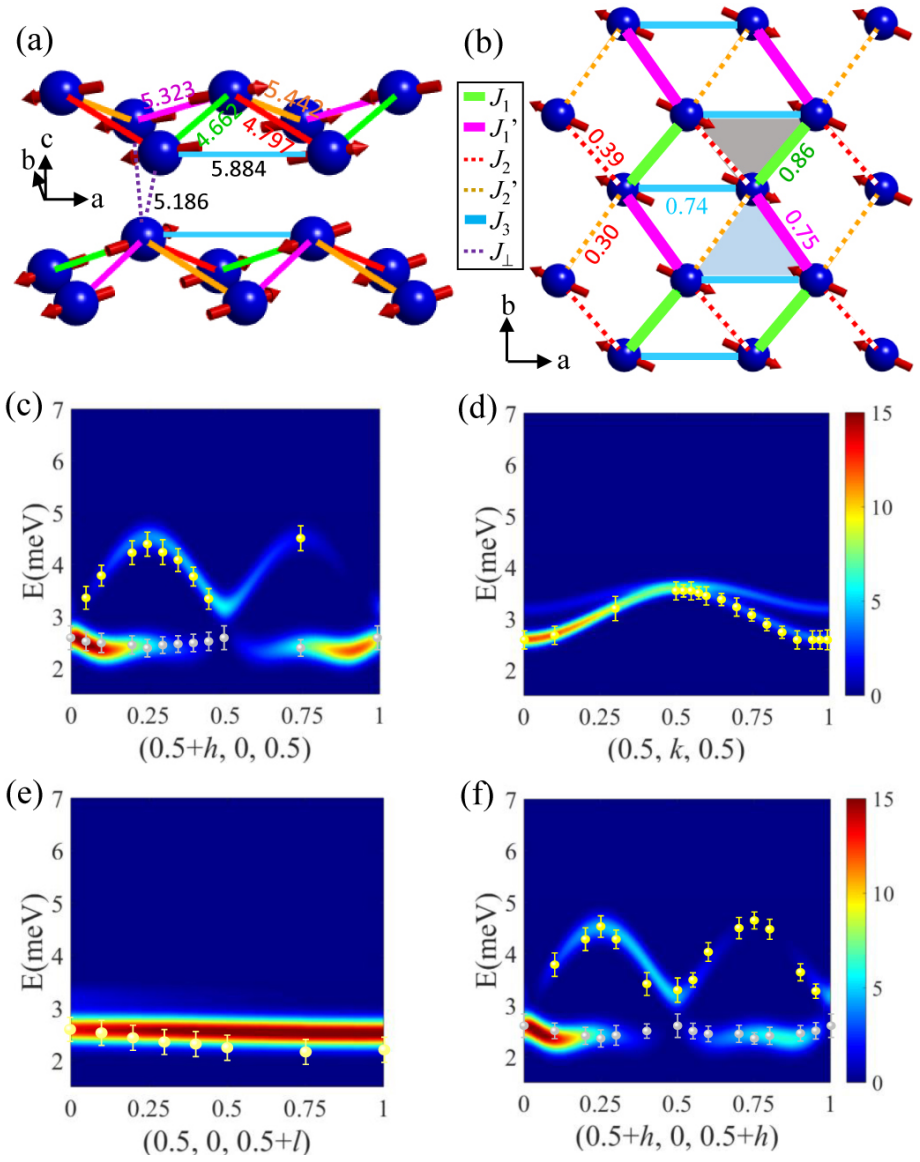

Fig. 3. (a) 3D illustration of Co-Co interaction network with spin configuration of two quasi CoO_4 PLSs [see Fig. 2(b)] with the Co NN distances. (b) The *ab*-plane projection of one quasi CoO_4 PLS showing Co-Co interactions, spin configurations with NN exchange parameters, buckled zigzag chains along the *b* axis, as well as the formed two triangular sublattices. (c)-(f) Simulated *S*(Q, E) spectra along the [*H* 0 0], [0 *K* 0], [0 0 *L*] and [*H* 0 *H*] directions in the r.l.u. using the magnetic exchange parameters obtained from the fits to the experimental SW dispersion and simulated intensity.

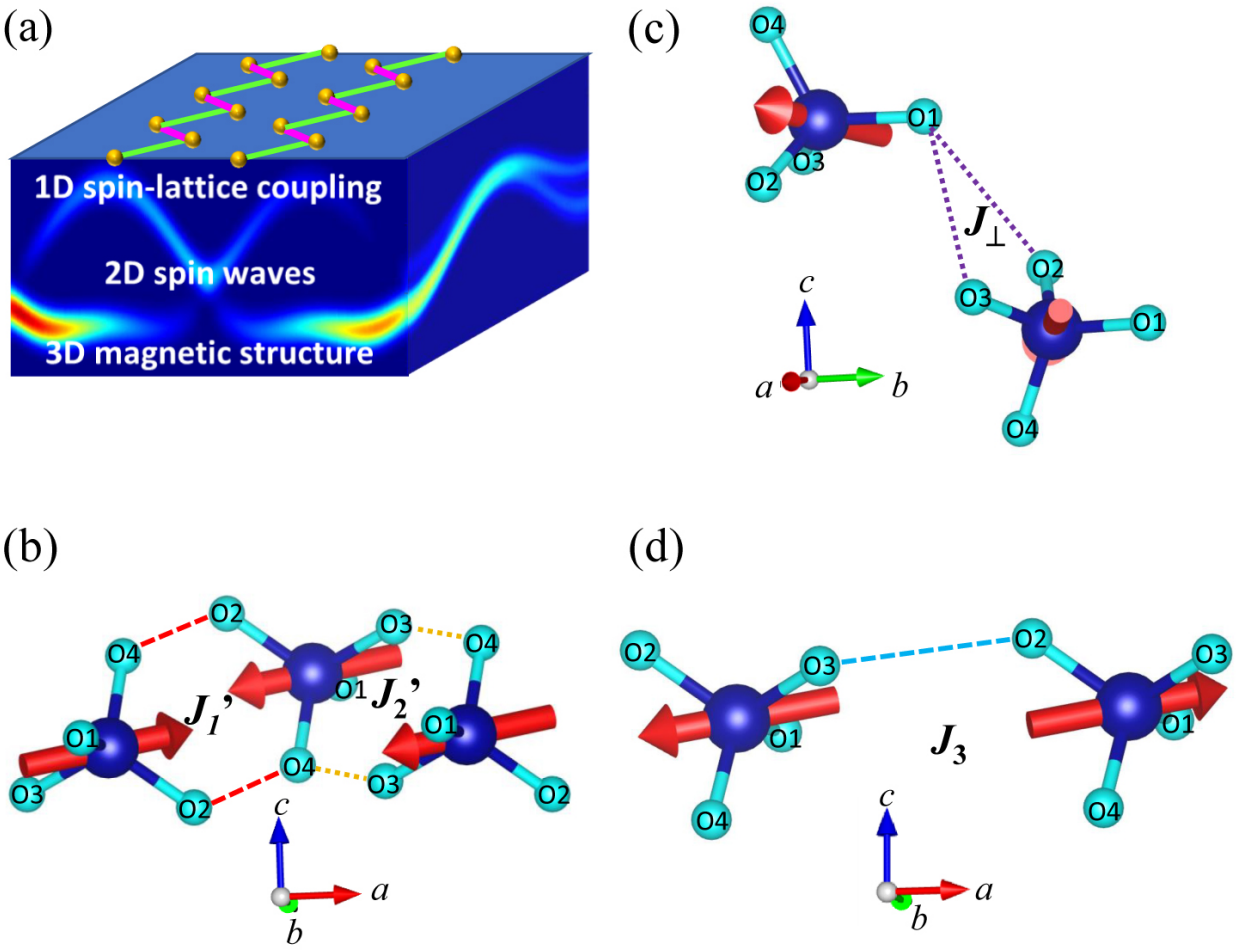

Fig. 4. (a) An illustrated view of different dimensional magnetism in Ba_2CoO_4. The zigzag magnetic chains are schematically shown. Geometrical representation of indirect spin exchange interaction paths of Co-O---O-Co associated with (b) inter-PLS NN interaction $J_\perp$, (c) intra-PLS NN interaction J_1' and J_2', (c) and (d) intra-PLS NNN interaction J_3 in Ba_2CoO_4.